



*Discrete Ordinates Radiation Transport using  
Higher-Order Finite Element Spatial Discretizations  
on Meshes with Curved Surfaces*

Dissertation Defense

Douglas N. Woods

4 June 2018

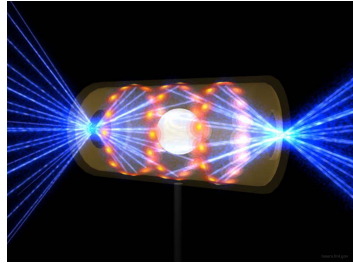
# Outline

- Introduction
- Objectives
- Methods
- MIP DSA
  - Implementation
  - Numerical Results
- *R-Z* Geometry
  - Implementation
  - Numerical Results
- Conclusions

# Introduction

## Radiation-hydrodynamics

- High energy density physics
  - astrophysics
  - inertial confinement fusion

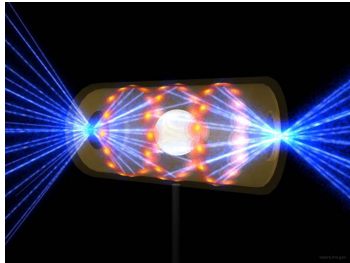


<https://lasers.llnl.gov/content/assets/images/media/photo-gallery/large/nif-1209-18059.jpg>

# Introduction

## Radiation-hydrodynamics

- High energy density physics
  - astrophysics
  - inertial confinement fusion
- Blackbody radiation can influence the energy, temperature, momentum, pressure of the fluid

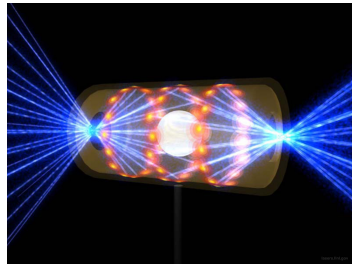


<https://lasers.llnl.gov/content/assets/images/media/photo-gallery/large/nif-1209-18059.jpg>

# Introduction

## Radiation-hydrodynamics

- High energy density physics
  - astrophysics
  - inertial confinement fusion
- Blackbody radiation can influence the energy, temperature, momentum, pressure of the fluid
- Radiation-hydrodynamics to study these problems

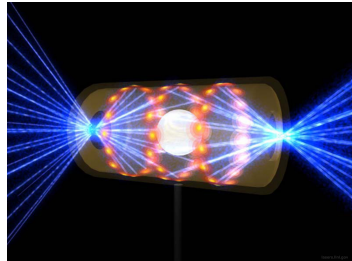


<https://lasers.llnl.gov/content/assets/images/media/photo-gallery/large/nif-1209-18059.jpg>

# Introduction

## Radiation-hydrodynamics

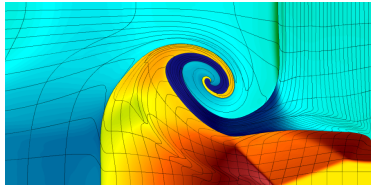
- High energy density physics
  - astrophysics
  - inertial confinement fusion
- Blackbody radiation can influence the energy, temperature, momentum, pressure of the fluid
- Radiation-hydrodynamics to study these problems
- Can study radiation transport and hydrodynamics separately



<https://lasers.llnl.gov/content/assets/images/media/photo-gallery/large/nif-1209-18059.jpg>

# Introduction

## BLAST — LLNL ALE hydrodynamics code



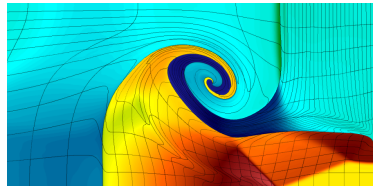
multi-material shock hydrodynamics problem solved with BLAST: 8<sup>th</sup>-order kinematics, 7<sup>th</sup>-order thermodynamics

<https://computation.llnl.gov/project/blast/>

- High-order (HO) finite element spatial discretization

# Introduction

## BLAST — LLNL ALE hydrodynamics code



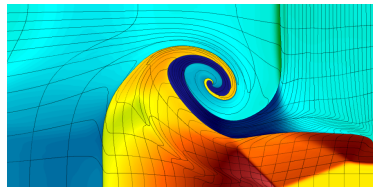
multi-material shock hydrodynamics problem solved with BLAST: 8<sup>th</sup>-order kinematics, 7<sup>th</sup>-order thermodynamics

<https://computation.llnl.gov/project/blast/>

- High-order (HO) finite element spatial discretization
- Meshes with curved surfaces
  - Straight-edged meshes restrict the accuracy of the compressible Euler equations
  - “Essential for higher-order accuracy”

# Introduction

## BLAST — LLNL ALE hydrodynamics code



multi-material shock hydrodynamics problem solved with BLAST: 8<sup>th</sup>-order kinematics, 7<sup>th</sup>-order thermodynamics

<https://computation.llnl.gov/project/blast/>

- High-order (HO) finite element spatial discretization
- Meshes with curved surfaces
  - Straight-edged meshes restrict the accuracy of the compressible Euler equations
  - “Essential for higher-order accuracy”
- More accurately model:
  - Fluid flow geometry in Lagrangian framework with curved meshes
  - Can model a shock front within a single zone - higher resolution
  - Radial flow symmetry

# Introduction

## High-order radiation transport

- HO ( $p \geq 2$ )  $S_N$  transport FEM research is relatively new
  - FEM approximates the solution to be a polynomial expansion
  - Low-order (LO) ( $p = 1$ ) methods are less computationally expensive
  - Expected spatial convergence of  $O(p + 1)$  have been shown
  - HO DFEMs are accurate in the diffusion limit
  - Some HO DFEM research in 1-D thermal radiation transport

# Introduction

## High-order radiation transport

- HO ( $p \geq 2$ )  $S_N$  transport FEM research is relatively new
  - FEM approximates the solution to be a polynomial expansion
  - Low-order (LO) ( $p = 1$ ) methods are less computationally expensive
  - Expected spatial convergence of  $O(p + 1)$  have been shown
  - HO DFEMs are accurate in the diffusion limit
  - Some HO DFEM research in 1-D thermal radiation transport
- R-Z geometry has only been explored using LO finite elements
  - 2<sup>nd</sup>-order spatial convergence for linear methods (BLD, PWLD, etc.)
  - Accurate in the diffusion limit

# Introduction

## High-order radiation transport

- HO ( $p \geq 2$ )  $S_N$  transport FEM research is relatively new
  - FEM approximates the solution to be a polynomial expansion
  - Low-order (LO) ( $p = 1$ ) methods are less computationally expensive
  - Expected spatial convergence of  $O(p + 1)$  have been shown
  - HO DFEMs are accurate in the diffusion limit
  - Some HO DFEM research in 1-D thermal radiation transport
- R-Z geometry has only been explored using LO finite elements
  - 2<sup>nd</sup>-order spatial convergence for linear methods (BLD, PWLD, etc.)
  - Accurate in the diffusion limit
- Structured/unstructured quadrilateral and triangular meshes
  - Some research for meshes with curved surfaces
  - Do not degrade  $O(p + 1)$  spatial convergence rate

# Objectives

- Use MFEM, a general finite element library ([mfem.org](http://mfem.org)):
  1. Modified interior penalty (MIP) diffusion synthetic acceleration (DSA)
    - Implement MIP DSA equations using homogeneous Robin (i.e. vacuum) boundary conditions
    - Examine and compare spectral radii to MIP DSA using homogeneous Dirichlet boundary conditions

# Objectives

- Use MFEM, a general finite element library ([mfem.org](http://mfem.org)):
  1. Modified interior penalty (MIP) diffusion synthetic acceleration (DSA)
    - Implement MIP DSA equations using homogeneous Robin (i.e. vacuum) boundary conditions
    - Examine and compare spectral radii to MIP DSA using homogeneous Dirichlet boundary conditions
  2. *R-Z* geometry
    - Numerically solve HO  $S_N$  transport equation on meshes with curved surfaces
    - Perform spatial convergence studies
    - Preserve 1-D spherical symmetry

# Methods

## HO DGFEM spatial discretization

- Steady-state, monoenergetic radiation transport equation

$$\begin{aligned}\Omega_m \cdot \nabla \psi_m + \sigma_t \psi_m &= \frac{1}{4\pi} \sigma_s \phi + \frac{1}{4\pi} S_0 \\ \phi &= \sum_m w_m \psi_m\end{aligned}$$

# Methods

## HO DGFEM spatial discretization

- Steady-state, monoenergetic radiation transport equation

$$\begin{aligned}\Omega_m \cdot \nabla \psi_m + \sigma_t \psi_m &= \frac{1}{4\pi} \sigma_s \phi + \frac{1}{4\pi} S_0 \\ \phi &= \sum_m w_m \psi_m\end{aligned}$$

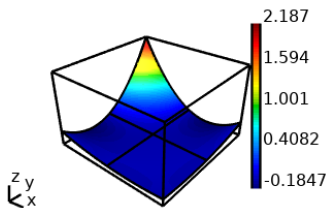
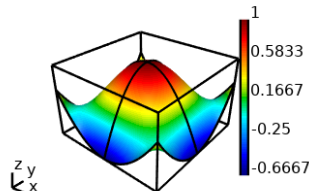
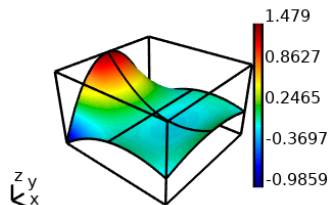
- Standard discontinuous Galerkin finite element method (DGFEM) spatial discretization

$$\begin{aligned}(\Omega_m \cdot \nabla \psi_m, v_i)_{\mathcal{D}_k} + (\sigma_t \psi_m, v_i)_{\mathcal{D}_k} &= \frac{1}{4\pi} (\sigma_s \phi, v_i)_{\mathcal{D}_k} + \frac{1}{4\pi} (S_0, v_i)_{\mathcal{D}_k} \\ \psi_m &\approx \sum_j b_j(\mathbf{x}) \psi_{j,m}\end{aligned}$$



# Methods

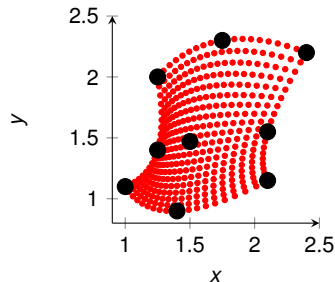
2<sup>nd</sup>-order basis functions allow for more complex solution shapes on each element



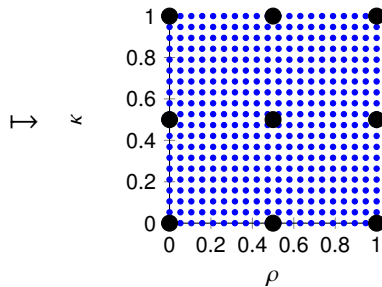
$$\begin{aligned} b_j(x, y) = & c_1 x^2 y^2 + c_2 x^2 y + c_3 x^2 \\ & + c_4 x y^2 + c_5 x y + c_6 x \\ & + c_7 y^2 + c_8 y + c_9 \end{aligned}$$

# Methods

HO mapping allows for meshes with curved surfaces



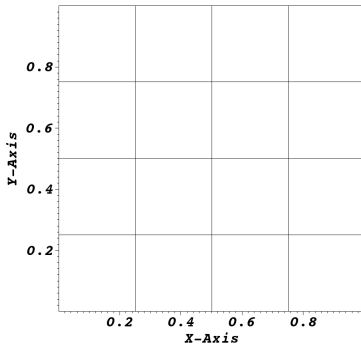
Physical element



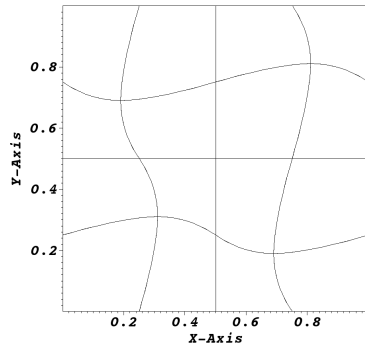
Reference element

# Methods

## HO mesh transformation example



Orthogonal mesh



3<sup>rd</sup>-order mesh

# Methods

Create DGFEM matrices using MFEM, solve using a direct solver

- MFEM generates local matrices and vectors for a variety of operators, assembles them into global linear algebra system
  - High-order finite elements
  - Create and transform meshes with curved surfaces

# Methods

Create DGFEM matrices using MFEM, solve using a direct solver

- MFEM generates local matrices and vectors for a variety of operators, assembles them into global linear algebra system
  - High-order finite elements
  - Create and transform meshes with curved surfaces
- Solve linear system directly with UMFPack  
(<http://faculty.cse.tamu.edu/davis/suitesparse.html>)
- Visualize solutions with VisIt  
(<https://wci.llnl.gov/simulation/computer-codes/visit>)

# Diffusion Synthetic Acceleration

## Source iteration acceleration

- Source iteration to solve radiation transport equation
  - Iterate on scalar flux until scattering source converges
  - Can converge arbitrarily slowly with increased scattering

$$\Omega \cdot \nabla \psi_m^{(\ell+1)} + \sigma_t \psi_m^{(\ell+1)} = \frac{1}{4\pi} \sigma_s \phi^{(\ell)} + \frac{1}{4\pi} S_0$$

$$\phi^{(\ell+1)} = \sum_m w_m \psi_m^{(\ell+1)}$$



# Diffusion Synthetic Acceleration

## Source iteration acceleration

- Source iteration to solve radiation transport equation
  - Iterate on scalar flux until scattering source converges
  - Can converge arbitrarily slowly with increased scattering

$$\Omega \cdot \nabla \psi_m^{(\ell+1)} + \sigma_t \psi_m^{(\ell+1)} = \frac{1}{4\pi} \sigma_s \phi^{(\ell)} + \frac{1}{4\pi} S_0$$

$$\phi^{(\ell+1)} = \sum_m w_m \psi_m^{(\ell+1)}$$

- Source iteration acceleration
  - Solve diffusion equation to make a small “correction” to the radiation transport solution

# Diffusion Synthetic Acceleration

## DSA algorithm

- Diffusion synthetic acceleration (DSA) algorithm

$$\Omega \cdot \nabla \psi_m^{(\ell+1/2)} + \sigma_t \psi_m^{(\ell+1/2)} = \frac{1}{4\pi} \sigma_s \phi^{(\ell)} + \frac{1}{4\pi} S_0$$
$$\phi^{(\ell+1/2)} = \sum_{m=1}^M w_m \psi_m^{(\ell+1/2)}$$

# Diffusion Synthetic Acceleration

## DSA algorithm

- Diffusion synthetic acceleration (DSA) algorithm

$$\Omega \cdot \nabla \psi_m^{(\ell+1/2)} + \sigma_t \psi_m^{(\ell+1/2)} = \frac{1}{4\pi} \sigma_s \phi^{(\ell)} + \frac{1}{4\pi} S_0$$

$$\phi^{(\ell+1/2)} = \sum_{m=1}^M w_m \psi_m^{(\ell+1/2)}$$

$$-\nabla \cdot D \nabla \varphi^{(\ell+1/2)} + \sigma_a \varphi^{(\ell+1/2)} = \sigma_s (\phi^{(\ell+1/2)} - \phi^{(\ell)})$$



# Diffusion Synthetic Acceleration

## DSA algorithm

- Diffusion synthetic acceleration (DSA) algorithm

$$\Omega \cdot \nabla \psi_m^{(\ell+1/2)} + \sigma_t \psi_m^{(\ell+1/2)} = \frac{1}{4\pi} \sigma_s \phi^{(\ell)} + \frac{1}{4\pi} S_0$$

$$\phi^{(\ell+1/2)} = \sum_{m=1}^M w_m \psi_m^{(\ell+1/2)}$$

$$-\nabla \cdot D \nabla \varphi^{(\ell+1/2)} + \sigma_a \varphi^{(\ell+1/2)} = \sigma_s (\phi^{(\ell+1/2)} - \phi^{(\ell)})$$

$$\phi^{(\ell+1)} = \phi^{(\ell+1/2)} + \varphi^{(\ell+1/2)}$$



# Modified Interior Penalty DSA

Implemented with homogeneous Dirichlet boundary conditions

- Wang and Ragusa (2010) derived modified interior penalty (MIP) DSA with homogeneous Dirichlet boundary conditions

# Modified Interior Penalty DSA

Implemented with homogeneous Dirichlet boundary conditions

- Wang and Ragusa (2010) derived modified interior penalty (MIP) DSA with homogeneous Dirichlet boundary conditions
- Bilinear form:

$$\begin{aligned} b_{MIP,D}(\varphi, v) = & (\sigma_a \varphi, v)_D + (D \nabla \varphi, \nabla v)_D \\ & + (\kappa_e [\![\varphi]\!], [\![v]\!])_{\partial D^i} + ([\![\varphi]\!], \{D \partial_n v\})_{\partial D^i} + (\{D \partial_n \varphi\}, [\![v]\!])_{\partial D^i} \\ & + (\kappa_e \varphi, v)_{\partial D^d} - \frac{1}{2} (\varphi, D \partial_n v)_{\partial D^d} - \frac{1}{2} (D \partial_n \varphi, v)_{\partial D^d} \end{aligned}$$

# Modified Interior Penalty DSA

Implemented with homogeneous Dirichlet boundary conditions

- Wang and Ragusa (2010) derived modified interior penalty (MIP) DSA with homogeneous Dirichlet boundary conditions
- Bilinear form:

$$\begin{aligned} b_{MIP,D}(\varphi, v) = & (\sigma_a \varphi, v)_D + (D \nabla \varphi, \nabla v)_D \\ & + (\kappa_e [\![\varphi]\!], [\![v]\!])_{\partial D^i} + ([\![\varphi]\!], \{D \partial_n v\})_{\partial D^i} + (\{D \partial_n \varphi\}, [\![v]\!])_{\partial D^i} \\ & + (\kappa_e \varphi, v)_{\partial D^d} - \frac{1}{2} (\varphi, D \partial_n v)_{\partial D^d} - \frac{1}{2} (D \partial_n \varphi, v)_{\partial D^d} \end{aligned}$$

- Linear form:

$$\ell_{MIP}(v) = \left( \sigma_s [\phi^{(\ell+1/2)} - \phi^{(\ell)}], v \right)_D$$

# Modified Interior Penalty DSA

Stabilization parameter is a function of an arbitrary coefficient

- “Switch” within the stabilization parameter between diffusion conforming form (DCF) and interior penalty (IP) method

$$\kappa_e = \max\left(\kappa_e^{IP}, \frac{1}{4}\right)$$

# Modified Interior Penalty DSA

Stabilization parameter is a function of an arbitrary coefficient

- “Switch” within the stabilization parameter between diffusion conforming form (DCF) and interior penalty (IP) method

$$\kappa_e = \max\left(\kappa_e^{IP}, \frac{1}{4}\right)$$

$$\kappa_e^{IP} = \begin{cases} \frac{f(p^+)}{2} \frac{D^+}{h_\perp^+} + \frac{f(p^-)}{2} \frac{D^-}{h_\perp^-}, & \text{on interior edges} \\ f(p) \frac{D}{h_\perp}, & \text{on boundary edges} \end{cases}$$

# Modified Interior Penalty DSA

Stabilization parameter is a function of an arbitrary coefficient

- “Switch” within the stabilization parameter between diffusion conforming form (DCF) and interior penalty (IP) method

$$\kappa_e = \max\left(\kappa_e^{IP}, \frac{1}{4}\right)$$

$$\kappa_e^{IP} = \begin{cases} \frac{f(p^+)}{2} \frac{D^+}{h_\perp^+} + \frac{f(p^-)}{2} \frac{D^-}{h_\perp^-}, & \text{on interior edges} \\ f(p) \frac{D}{h_\perp}, & \text{on boundary edges} \end{cases}$$

$$f(p) = C p(p+1)$$

# Modified Interior Penalty DSA

Stabilization parameter is a function of an arbitrary coefficient

- “Switch” within the stabilization parameter between diffusion conforming form (DCF) and interior penalty (IP) method

$$\kappa_e = \max\left(\kappa_e^{IP}, \frac{1}{4}\right)$$

$$\kappa_e^{IP} = \begin{cases} \frac{f(p^+)}{2} \frac{D^+}{h_\perp^+} + \frac{f(p^-)}{2} \frac{D^-}{h_\perp^-}, & \text{on interior edges} \\ f(p) \frac{D}{h_\perp}, & \text{on boundary edges} \end{cases}$$

$$f(p) = C p(p+1)$$

- $C$  is an arbitrary constant (i.e. 2, 4, 6)

# Modified Interior Penalty DSA

Implemented with homogeneous Robin boundary conditions

- We modify the MIP DSA equations to include homogeneous Robin boundary conditions
  - Dirichlet BC fixes boundary solution to  $\varphi = 0$
  - Robin BC is a true vacuum boundary condition
- Implement the boundary condition:

$$0 = \frac{1}{4}\varphi + \frac{1}{2}D\boldsymbol{\nabla}\varphi \cdot \hat{\mathbf{n}}$$

# Modified Interior Penalty DSA

Implemented with homogeneous Robin boundary conditions

- We modify the MIP DSA equations to include homogeneous Robin boundary conditions
  - Dirichlet BC fixes boundary solution to  $\varphi = 0$
  - Robin BC is a true vacuum boundary condition
- Implement the boundary condition:

$$0 = \frac{1}{4}\varphi + \frac{1}{2}D\boldsymbol{\nabla}\varphi \cdot \hat{n}$$

$$-(\boldsymbol{\nabla} \cdot D\boldsymbol{\nabla}\varphi, v)_{\mathcal{D}} = (D\boldsymbol{\nabla}\varphi, \boldsymbol{\nabla}v)_{\mathcal{D}} - (D\boldsymbol{\nabla}\varphi \cdot \hat{n}, v)_{\partial\mathcal{D}}$$

# Modified Interior Penalty DSA

Implemented with homogeneous Robin boundary conditions

- We modify the MIP DSA equations to include homogeneous Robin boundary conditions
  - Dirichlet BC fixes boundary solution to  $\varphi = 0$
  - Robin BC is a true vacuum boundary condition
- Implement the boundary condition:

$$0 = \frac{1}{4}\varphi + \frac{1}{2}D\boldsymbol{\nabla}\varphi \cdot \hat{n}$$

$$-(\boldsymbol{\nabla} \cdot D\boldsymbol{\nabla}\varphi, v)_{\mathcal{D}} = (D\boldsymbol{\nabla}\varphi, \boldsymbol{\nabla}v)_{\mathcal{D}} - (D\boldsymbol{\nabla}\varphi \cdot \hat{n}, v)_{\partial\mathcal{D}}$$

$$-(\boldsymbol{\nabla} \cdot D\boldsymbol{\nabla}\varphi, v)_{\mathcal{D}} = (D\boldsymbol{\nabla}\varphi, \boldsymbol{\nabla}v)_{\mathcal{D}} - (D\boldsymbol{\nabla}\varphi \cdot \hat{n}, v)_{\partial\mathcal{D}^i} - (D\boldsymbol{\nabla}\varphi \cdot \hat{n}, v)_{\partial\mathcal{D}^d}$$



# Modified Interior Penalty DSA

Implemented with homogeneous Robin boundary conditions

- We modify the MIP DSA equations to include homogeneous Robin boundary conditions
  - Dirichlet BC fixes boundary solution to  $\varphi = 0$
  - Robin BC is a true vacuum boundary condition
- Implement the boundary condition:

$$0 = \frac{1}{4}\varphi + \frac{1}{2}D\boldsymbol{\nabla}\varphi \cdot \hat{n}$$

- Bilinear form:

$$\begin{aligned} b_{MIP,R}(\varphi, v) &= (\sigma_a \varphi, v)_{\mathcal{D}} + (D \boldsymbol{\nabla}\varphi, \boldsymbol{\nabla}v)_{\mathcal{D}} \\ &+ (\kappa_e [\![\varphi]\!], [\![v]\!])_{\partial\mathcal{D}^i} + ([\![\varphi]\!], \{D \partial_n v\})_{\partial\mathcal{D}^i} + (\{D \partial_n \varphi\}, [\![v]\!])_{\partial\mathcal{D}^i} \\ &+ \left( \frac{1}{2}\varphi, v \right)_{\partial\mathcal{D}^d} \end{aligned}$$



# MIP DSA Sensitivity Study

Sensitivity of spectral radius to element order  $p$ , constant  $C$ , DSA boundary condition

- Wang and Ragusa studied convergence rates of their MIP DSA formulation
- Sensitivity studies on the spectral radius for
  - Finite element order  $p$
  - Varying the constant  $C$  (part of the stabilization parameter  $\kappa_e$ ) of the MIP DSA equations
  - Homogeneous Dirichlet versus Robin boundary conditions

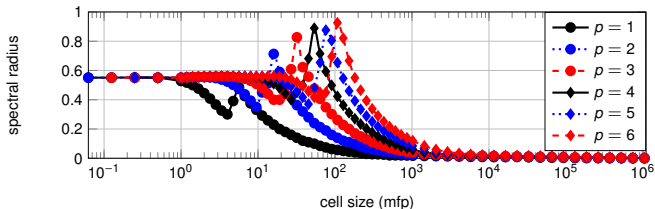
# MIP DSA Sensitivity Study

Sensitivity of spectral radius to element order  $p$ , constant  $C$ , DSA boundary condition

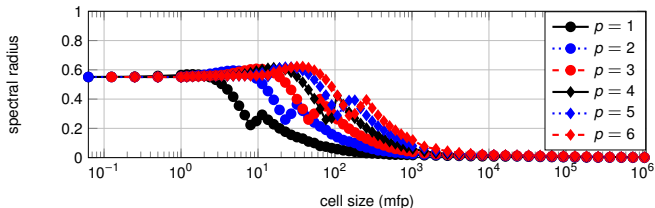
- Wang and Ragusa studied convergence rates of their MIP DSA formulation
- Sensitivity studies on the spectral radius for
  - Finite element order  $p$
  - Varying the constant  $C$  (part of the stabilization parameter  $\kappa_e$ ) of the MIP DSA equations
  - Homogeneous Dirichlet versus Robin boundary conditions
- Problem description:
  - 10x10 zoned mesh on unit square
  - Vacuum boundaries
  - Scattering ratio  $c = 0.9999$
  - Total cross section  $\sigma_t$  selected at run time to establish cell size

# MIP DSA Sensitivity Study

Unconditionally converges with homogeneous Dirichlet boundary conditions



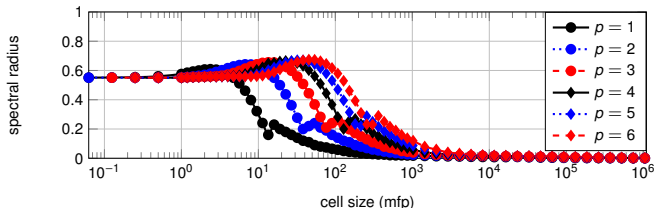
Spectral radius data for varying  $p$  with  $C = 2$ .



Spectral radius data for varying  $p$  with  $C = 4$ .

# MIP DSA Sensitivity Study

Unconditionally converges with homogeneous Dirichlet boundary conditions

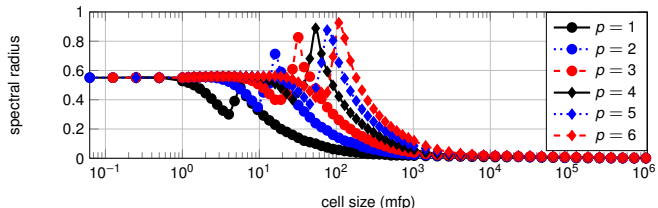


Spectral radius data for varying  $p$  with  $C = 6$ .

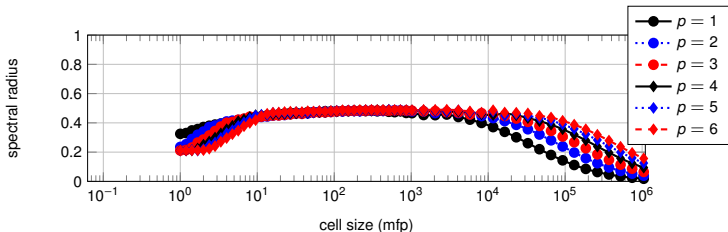
- Our 1<sup>st</sup>-order,  $C = 2$  results resemble Wang and Ragusa's results
- Unconditionally converging (spectral radius less than 1)
- Substantial dependence on  $C$  and  $p$
- Orthogonal and 3<sup>rd</sup>-order meshes exhibit similar behavior

# MIP DSA Sensitivity Study

Unconditionally converges with homogeneous Robin boundary conditions



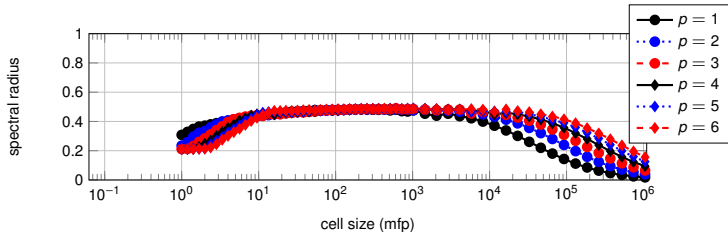
Spectral radius data for varying  $p$  with  $C = 2$  (Dirichlet BC repeated).



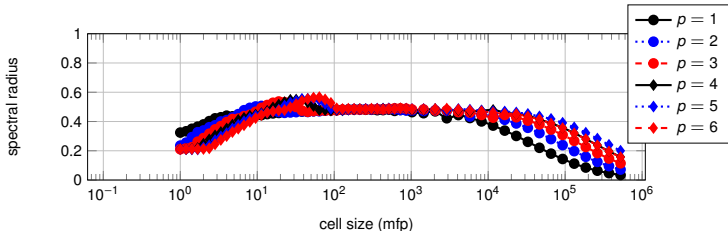
Spectral radius data for varying  $p$  with  $C = 2$ .

# MIP DSA Sensitivity Study

Unconditionally converges with homogeneous Robin boundary conditions



Spectral radius data for varying  $p$  with  $C = 4$ .



Spectral radius data for varying  $p$  with  $C = 6$ .

# MIP DSA Sensitivity Study

Unconditionally converges with homogeneous Robin boundary conditions

- Unconditionally convergent (spectral radius less than 1)
- Much less dependence on  $C$  and  $p$
- Intermediate cell sizes have smoother profiles than Dirichlet boundary conditions
- Optically thick regime converges slower than Dirichlet boundary conditions
- Heterogeneous problems degrade MIP DSA performance

# R-Z Geometry

Streaming term introduces an angular derivative

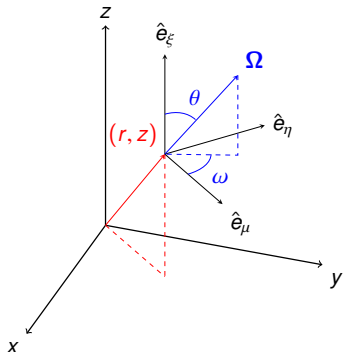
$$\frac{\mu}{r} \frac{\partial}{\partial r} (r \psi) + \xi \frac{\partial}{\partial z} \psi - \frac{1}{r} \frac{\partial}{\partial \omega} (\eta \psi) + \sigma_t \psi = \frac{1}{2\pi} \sigma_s \phi + \frac{1}{2\pi} S_0$$

$$\mu = \sqrt{1 - \xi^2} \cos(\omega)$$

$$\eta = \sqrt{1 - \xi^2} \sin(\omega)$$

$$\xi = \cos(\theta)$$

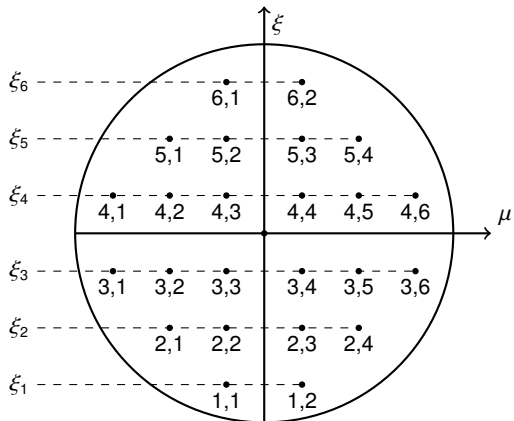
- Direction coordinate axes change with position
- $\hat{e}_\mu$  is always in  $r$ -direction



# R-Z Geometry

## Level symmetric angular quadrature

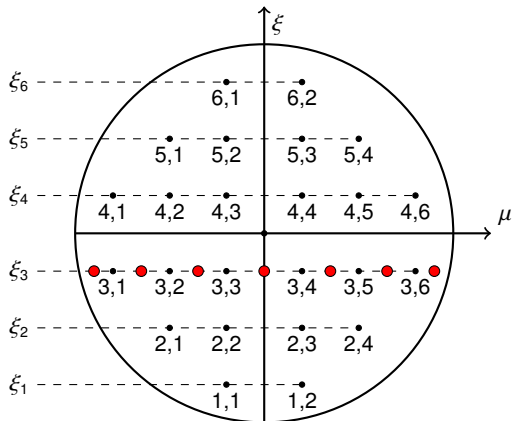
- Angular discretization showing  $(\xi_n, \mu_{n,m})$  pairs



# R-Z Geometry

## Level symmetric angular quadrature

- Angular discretization showing  $(\xi_n, \mu_{n,m})$  pairs



# R-Z Geometry

Angular derivative approximation - Morel and Montry

$$-\frac{1}{r} \frac{\partial}{\partial \omega} \eta_{n,m} \psi_{n,m}(r, z, \Omega) = \frac{\alpha_{m+1/2}^n \psi_{n,m+1/2} - \alpha_{m-1/2}^n \psi_{n,m-1/2}}{r w_{n,m}}$$

# R-Z Geometry

## Angular derivative approximation - Morel and Montry

$$-\frac{1}{r} \frac{\partial}{\partial \omega} \eta_{n,m} \psi_{n,m}(r, z, \Omega) = \frac{\alpha_{m+1/2}^n \psi_{n,m+1/2} - \alpha_{m-1/2}^n \psi_{n,m-1/2}}{r w_{n,m}}$$

- Define angular differencing coefficients to preserve uniform infinite medium solution (i.e.,  $\Omega \cdot \nabla \psi = 0$ )

$$\alpha_{m+1/2}^n = \alpha_{m-1/2}^n - \mu_{n,m} w_{n,m}$$

$$\alpha_{1/2}^n = \alpha_{M_n+1/2}^n = 0$$



# R-Z Geometry

## Angular derivative approximation - Morel and Montry

- Weighted diamond difference approximation for  $\psi_{n,m}$  between  $\psi_{n,m-1/2}$  and  $\psi_{n,m+1/2}$ , angular fluxes at the boundary of the discrete ordinate direction

$$\begin{aligned}\psi_{n,m} &= \tau_{n,m}\psi_{n,m+1/2} + (1 - \tau_{n,m})\psi_{n,m-1/2} \\ \tau_{n,m} &= \frac{\mu_{n,m} - \mu_{n,m+1/2}}{\mu_{n,m+1/2} - \mu_{n,m-1/2}}\end{aligned}$$

# R-Z Geometry

## Angular derivative approximation - Morel and Montry

- Weighted diamond difference approximation for  $\psi_{n,m}$  between  $\psi_{n,m-1/2}$  and  $\psi_{n,m+1/2}$ , angular fluxes at the boundary of the discrete ordinate direction

$$\psi_{n,m} = \tau_{n,m} \psi_{n,m+1/2} + (1 - \tau_{n,m}) \psi_{n,m-1/2}$$

$$\tau_{n,m} = \frac{\mu_{n,m} - \mu_{n,m+1/2}}{\mu_{n,m+1/2} - \mu_{n,m-1/2}}$$

$$\mu_{n,m+1/2} = \sqrt{1 - \xi_n^2} \cos(\gamma_{n,m+1/2})$$

$$\gamma_{n,m+1/2} = \gamma_{n,m-1/2} + \frac{\pi w_{n,m}}{\sum_{m=1}^{M_n} w_{n,m}}$$

$$\gamma_{n,1/2} = -\pi$$

# R-Z Geometry

## Angular derivative approximation - Morel and Montry

- Solve for starting directions  $\psi_{n,1/2}$  using Cartesian geometry transport equation

$$\boldsymbol{\Omega} \cdot \nabla \psi_{n,1/2} + \sigma_t \psi_{n,1/2} = \frac{1}{2\pi} \sigma_s \phi + \frac{1}{2\pi} S_0$$

# R-Z Geometry

## Angular derivative approximation - Morel and Montry

- Solve for starting directions  $\psi_{n,1/2}$  using Cartesian geometry transport equation

$$\Omega \cdot \nabla \psi_{n,1/2} + \sigma_t \psi_{n,1/2} = \frac{1}{2\pi} \sigma_s \phi + \frac{1}{2\pi} S_0$$

- Relate the starting direction ( $m = 1/2$ ) to the first discrete ordinates direction ( $m = 1$ )

$$\psi_{n,1} = \tau_{n,1} \psi_{n,1+1/2} + (1 - \tau_{n,1}) \psi_{n,1/2}$$

# R-Z Geometry

## Angular derivative approximation - Morel and Montry

- Solve for starting directions  $\psi_{n,1/2}$  using Cartesian geometry transport equation

$$\boldsymbol{\Omega} \cdot \nabla \psi_{n,1/2} + \sigma_t \psi_{n,1/2} = \frac{1}{2\pi} \sigma_s \phi + \frac{1}{2\pi} S_0$$

- Relate the starting direction ( $m = 1/2$ ) to the first discrete ordinates direction ( $m = 1$ )

$$\begin{aligned}\psi_{n,1} &= \tau_{n,1} \psi_{n,1+1/2} + (1 - \tau_{n,1}) \psi_{n,1/2} \\ - \frac{1}{r} \frac{\partial}{\partial \omega} \eta \psi &= \frac{\alpha_{1+1/2}^n \psi_{n,1+1/2} - \alpha_{1/2}^n \psi_{n,1/2}}{r w_{n,1}}\end{aligned}$$

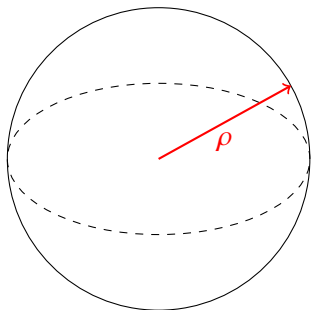


# Axisymmetry Preservation

Preserve 1-D spherical symmetry using *R-Z* geometry

- Preserve 1-D spherical symmetry
  - only a function of spherical radius,  $\rho$

$$\rho \equiv \sqrt{r^2 + z^2}$$

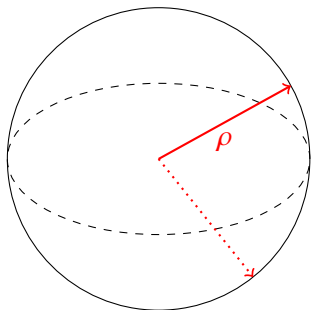


# Axisymmetry Preservation

Preserve 1-D spherical symmetry using *R-Z* geometry

- Preserve 1-D spherical symmetry
  - only a function of spherical radius,  $\rho$

$$\rho \equiv \sqrt{r^2 + z^2}$$

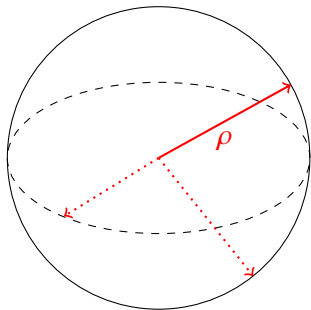


# Axisymmetry Preservation

Preserve 1-D spherical symmetry using *R-Z* geometry

- Preserve 1-D spherical symmetry
  - only a function of spherical radius,  $\rho$

$$\rho \equiv \sqrt{r^2 + z^2}$$

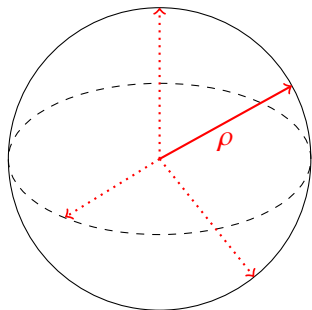


# Axisymmetry Preservation

Preserve 1-D spherical symmetry using *R-Z* geometry

- Preserve 1-D spherical symmetry
  - only a function of spherical radius,  $\rho$

$$\rho \equiv \sqrt{r^2 + z^2}$$

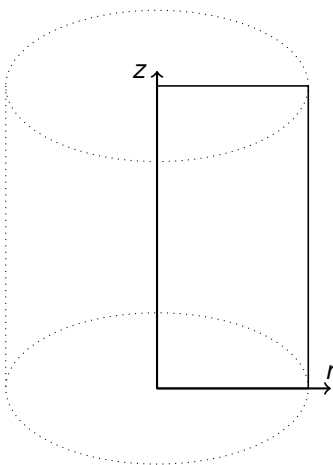
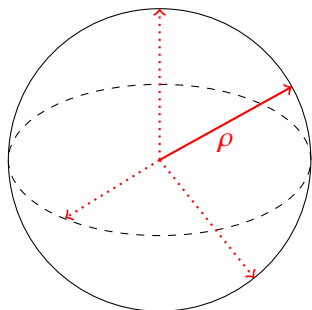


# Axisymmetry Preservation

Preserve 1-D spherical symmetry using *R-Z* geometry

- Preserve 1-D spherical symmetry
  - only a function of spherical radius,  $\rho$

$$\rho \equiv \sqrt{r^2 + z^2}$$

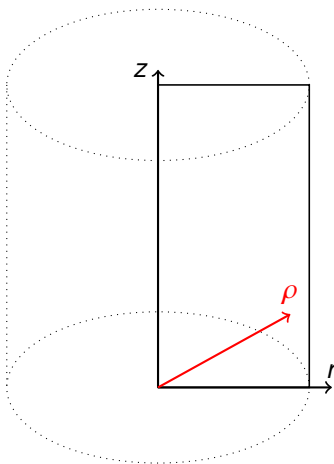
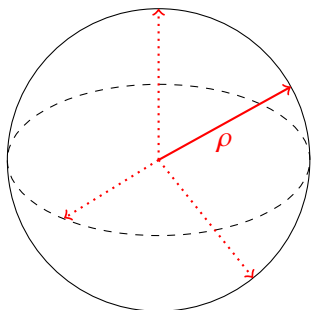


# Axisymmetry Preservation

Preserve 1-D spherical symmetry using *R-Z* geometry

- Preserve 1-D spherical symmetry
  - only a function of spherical radius,  $\rho$

$$\rho \equiv \sqrt{r^2 + z^2}$$

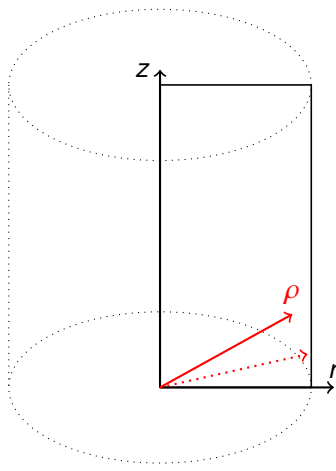
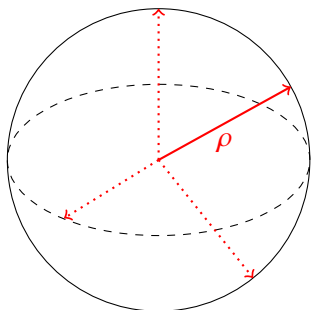


# Axisymmetry Preservation

Preserve 1-D spherical symmetry using *R-Z* geometry

- Preserve 1-D spherical symmetry
  - only a function of spherical radius,  $\rho$

$$\rho \equiv \sqrt{r^2 + z^2}$$

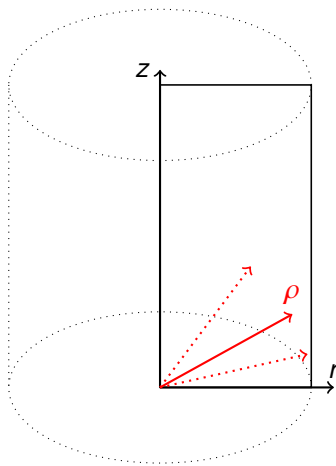
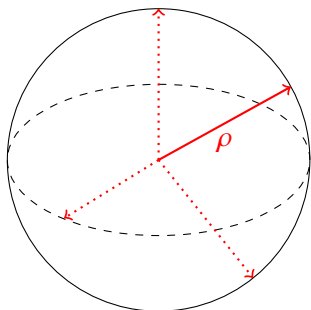


# Axisymmetry Preservation

Preserve 1-D spherical symmetry using *R-Z* geometry

- Preserve 1-D spherical symmetry
  - only a function of spherical radius,  $\rho$

$$\rho \equiv \sqrt{r^2 + z^2}$$



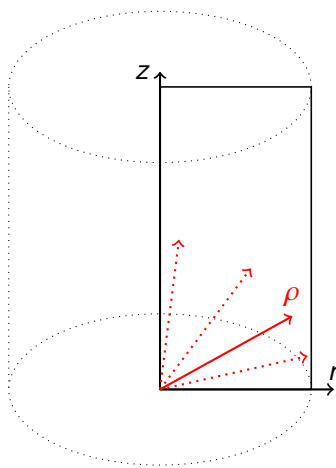
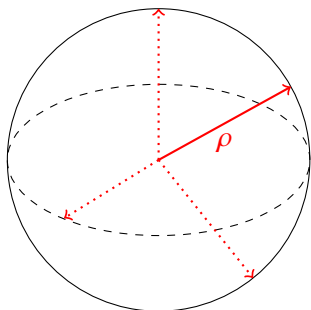
Oregon State  
University

# Axisymmetry Preservation

Preserve 1-D spherical symmetry using *R-Z* geometry

- Preserve 1-D spherical symmetry
  - only a function of spherical radius,  $\rho$

$$\rho \equiv \sqrt{r^2 + z^2}$$



Oregon State  
University

# Axisymmetry Preservation

Preserve 1-D spherical symmetry using *R-Z* geometry

- Solve MMS problem with manufactured solution:

$$\psi_{\text{MMS}} = \rho \equiv \sqrt{r^2 + z^2}$$

- Homogeneous material with  $\sigma_t = 5.0$ ,  $\sigma_s = 2.0$
- Incident angular flux on  $\rho = 1$  boundary
- Reflecting boundary at  $r = 0$
- $p = \{1, 2, 4, 8\}$ , several  $S_N$  orders ( $N = \{4, 6, 8, 10, 12\}$ ), 1<sup>st</sup>- and 2<sup>nd</sup>-order meshes, several mesh refinements

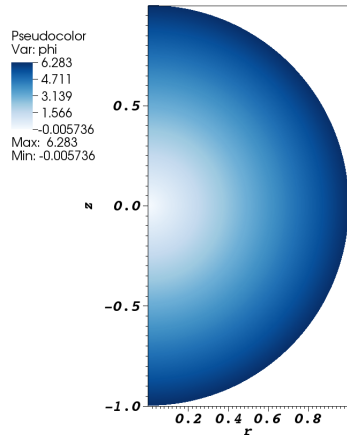
# Axisymmetry Preservation

Preserve 1-D spherical symmetry using *R-Z* geometry

- Solve MMS problem with manufactured solution:

$$\psi_{\text{MMS}} = \rho \equiv \sqrt{r^2 + z^2}$$

- Homogeneous material with  $\sigma_t = 5.0, \sigma_s = 2.0$
- Incident angular flux on  $\rho = 1$  boundary
- Reflecting boundary at  $r = 0$
- $p = \{1, 2, 4, 8\}$ , several  $S_N$  orders ( $N = \{4, 6, 8, 10, 12\}$ ), 1<sup>st</sup>- and 2<sup>nd</sup>-order meshes, several mesh refinements



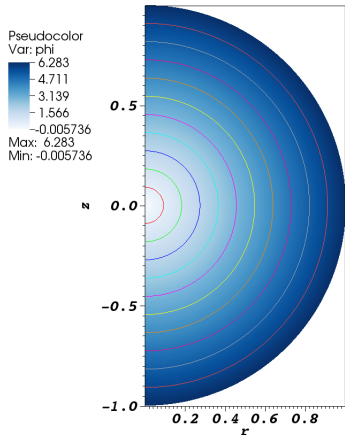
# Axisymmetry Preservation

Preserve 1-D spherical symmetry using  $R$ - $Z$  geometry

- Solve MMS problem with manufactured solution:

$$\psi_{\text{MMS}} = \rho \equiv \sqrt{r^2 + z^2}$$

- Homogeneous material with  $\sigma_t = 5.0$ ,  $\sigma_s = 2.0$
- Incident angular flux on  $\rho = 1$  boundary
- Reflecting boundary at  $r = 0$
- $p = \{1, 2, 4, 8\}$ , several  $S_N$  orders ( $N = \{4, 6, 8, 10, 12\}$ ), 1<sup>st</sup>- and 2<sup>nd</sup>-order meshes, several mesh refinements



# Axisymmetry Preservation

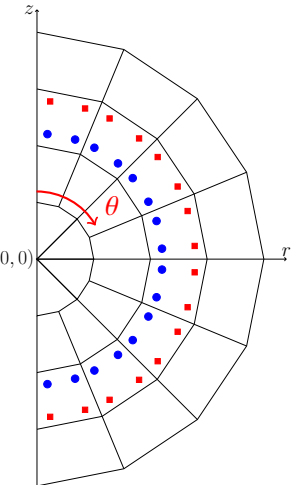
Preserve 1-D spherical symmetry using *R-Z* geometry

- Compare each nodal solution to the average solution at each spherical radius  
 $\rho = \sqrt{r^2 + z^2}$

$$\phi_{\text{asym}}(\rho) = \left| \frac{\phi_{\text{DFEM}}(\rho, \theta) - \phi_{\text{avg}}(\rho)}{\phi_{\text{avg}}(\rho)} \right|$$

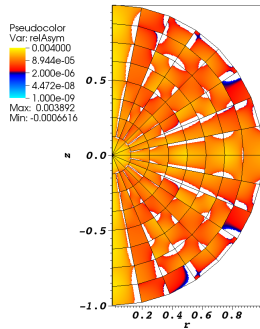
$$\phi_{\text{avg}}(\rho) = \frac{1}{N_{\text{nodes}}(\rho)} \sum_{i=1}^{N_{\text{nodes}}(\rho)} \phi_{\text{DFEM}}(\rho, \theta_i)$$

- Plot the FEM “shape” of  $\phi_{\text{asym}}$

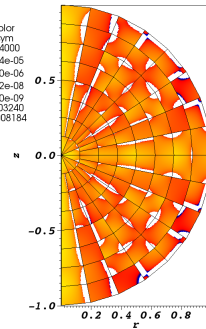


# Axisymmetry Preservation

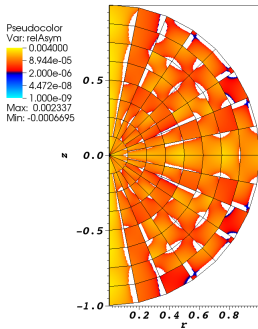
Relative asymmetry for 1<sup>st</sup>-order finite elements on a 1<sup>st</sup>-order mesh for given order of level-symmetric angular quadrature



(a)  $S_4$



(b)  $S_8$

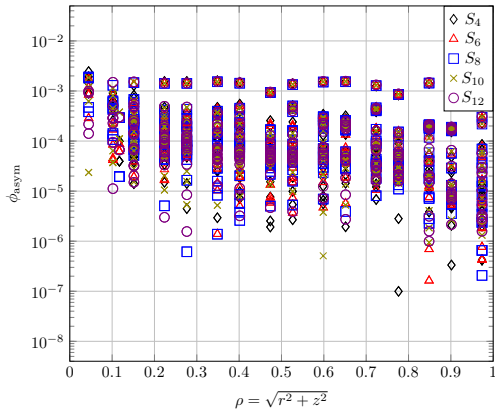


(c)  $S_{12}$

# Axisymmetry Preservation

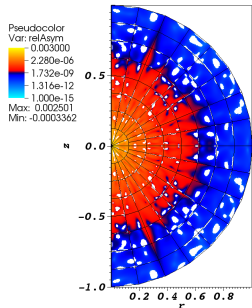
Relative asymmetry for 1<sup>st</sup>-order finite elements on a 1<sup>st</sup>-order mesh for given order of level-symmetric angular quadrature

- Difficult to distinguish between  $S_N$  solutions
- Greatest asymmetry near origin
- Asymmetry reaches an asymptotic value  $\sim 10^{-3}$
- Accuracy of solution is nearly constant

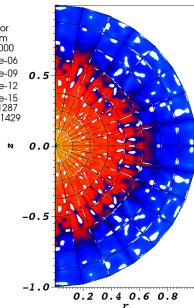


# Axisymmetry Preservation

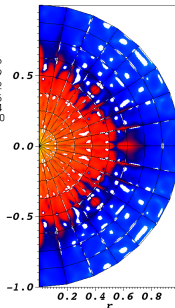
Relative asymmetry for 4<sup>th</sup>-order finite elements on a 1<sup>st</sup>-order mesh for given order of level-symmetric angular quadrature



(a)  $S_4$



(b)  $S_8$

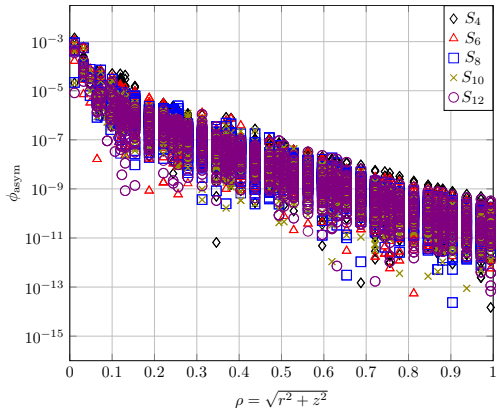


(c)  $S_{12}$

# Axisymmetry Preservation

Relative asymmetry for 4<sup>th</sup>-order finite elements on a 1<sup>st</sup>-order mesh for given order of level-symmetric angular quadrature

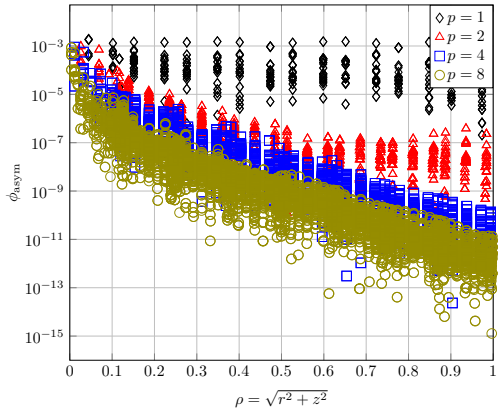
- Difficult to distinguish between  $S_N$  solutions
- Greatest asymmetry near origin
- Asymmetry does not reach an asymptotic value ( $< 10^{-9}$ )
- Accuracy of solution is nearly constant



# Axisymmetry Preservation

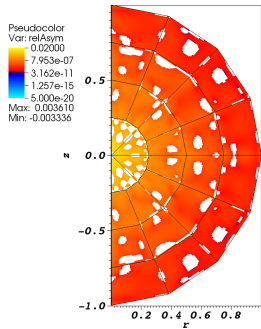
Relative asymmetries for each finite element order on a 1<sup>st</sup>-order mesh for  $S_8$  level-symmetric angular quadrature

- 1<sup>st</sup>- and 2<sup>nd</sup>-order finite elements reach asymptotic asymmetry
- Increasing finite element order increases relative symmetry
- Asymmetry does not reach an asymptotic value ( $< 10^{-9}$ ) for higher-order finite elements
- Relative symmetry is nearly identical at the origin

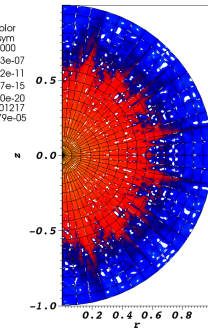


# Axisymmetry Preservation

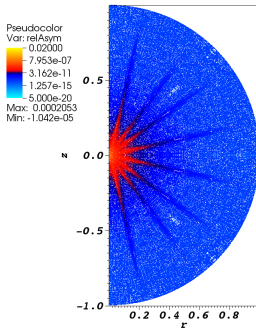
Relative asymmetry under spatial refinement for 4<sup>th</sup>-order finite elements on a 1<sup>st</sup>-order mesh for given order of level-symmetric angular quadrature



(a) 28 zones



(b) 496 zones

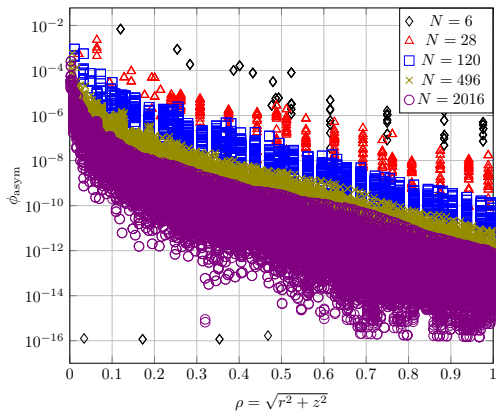


(c) 8128 zones

# Axisymmetry Preservation

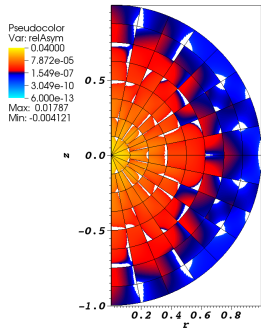
Relative asymmetries under spatial refinement for 4<sup>st</sup>-order finite elements on a 1<sup>st</sup>-order mesh for  $S_8$  level-symmetric angular quadrature

- Mesh refinement increases symmetry preservation
- Largest magnitude asymmetries are located near the origin
- Mesh refinement increases accuracy of scalar flux

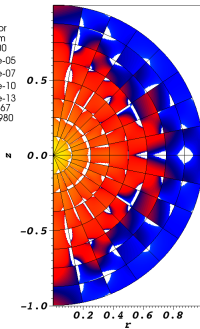


# Axisymmetry Preservation

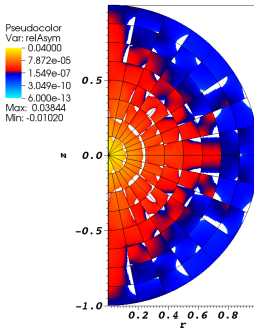
Relative asymmetry for 1<sup>st</sup>-order finite elements on a 2<sup>nd</sup>-order mesh for given order of level-symmetric angular quadrature



(a)  $S_4$



(b)  $S_8$

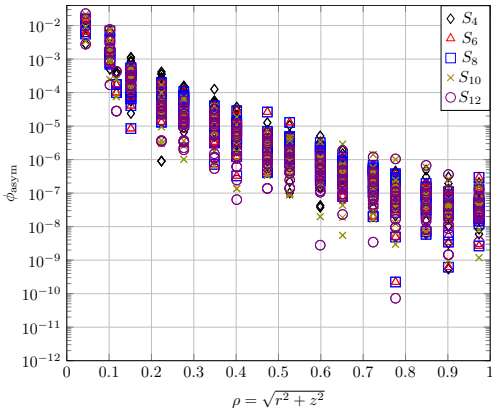


(c)  $S_{12}$

# Axisymmetry Preservation

Relative asymmetry for 1<sup>st</sup>-order finite elements on a 2<sup>nd</sup>-order mesh for given order of level-symmetric angular quadrature

- Difficult to distinguish between  $S_N$  solutions
- Greatest asymmetry near origin
- Asymmetry does not reach an asymptotic value ( $< 10^{-6}$ )
- Accuracy is nearly constant



# MIP DSA Conclusions

- Implemented MIP DSA equations with Robin boundary conditions
  - Unconditionally converging
  - Greatly accelerates source iteration
- Compared spectral radii to the MIP DSA equations with Dirichlet boundary conditions
  - Robin BCs do not generate the peaks
  - Robin BCs are not as dependent on the constant  $C$  or  $p$
  - Robin BCs have significantly higher spectral radii in optically thick region
- Future work
  - Investigate the optically thick region
  - Fourier analysis
  - Implement MIP DSA in a preconditioned Krylov method

# R-Z Geometry Conclusions

- Implemented and characterized the *R-Z* spatial discretization using HO finite elements on meshes with curved surfaces
- Observed expected  $O(p + 1)$  spatial convergence rates on smooth solutions
- Curvature of the mesh does not degrade spatial convergence
- Axisymmetry preservation is conditional with two dominant factors:
  - spatial mesh refinement
  - finite element order
- Future work
  - Numerically demonstrate diffusion limit
  - Consider alternate derivations of *R-Z* equations
  - Consider other manufactured solutions and materials for symmetry preservation

# Thank you!



Oregon State  
University

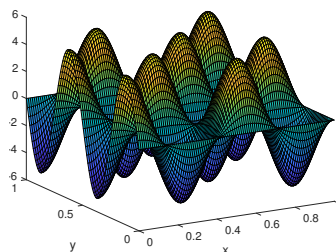
# X-Y Geometry

## Spatial convergence study

- Method of manufactured solutions (MMS) to determine convergence rates

$$\psi_{\text{MMS}} = (1 - \mu^2)(1 - \eta^2) \sin(4\pi x) \cos\left(\frac{7}{2}\pi y\right)$$

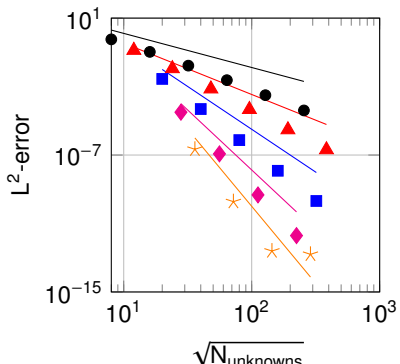
- Calculate  $\|\phi_{\text{code}} - \phi_{\text{MMS}}\|_{L^2}$  for sequential mesh refinements
- Use  $p = \{1, 2, 4, 6, 8\}$
- Orthogonal and 3<sup>rd</sup>-order meshes



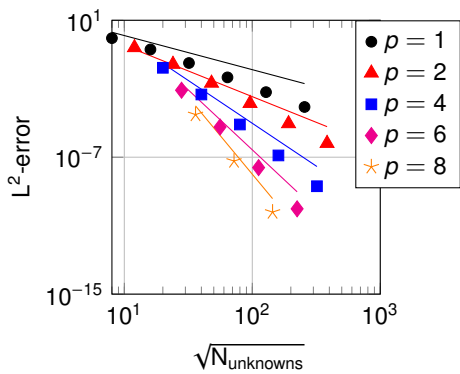
# X-Y Geometry

Spatial convergence study shows  $p + 1$  convergence

- $N_{\text{unknowns}} = N_{\text{cells}}(p + 1)^2$
- Reference lines show  $p + 1$  spatial convergences



Orthogonal mesh



3<sup>rd</sup>-order mesh



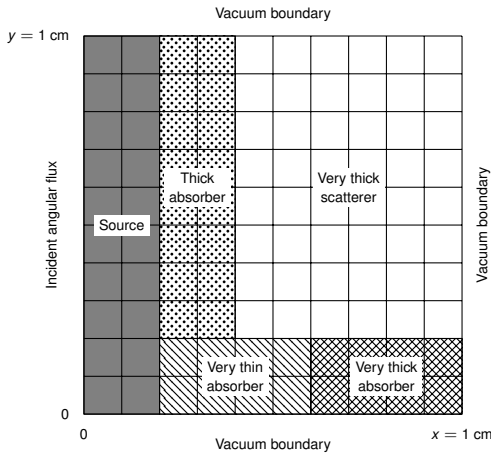
Oregon State  
University

# X-Y Geometry

## Strong material heterogeneity problem definition

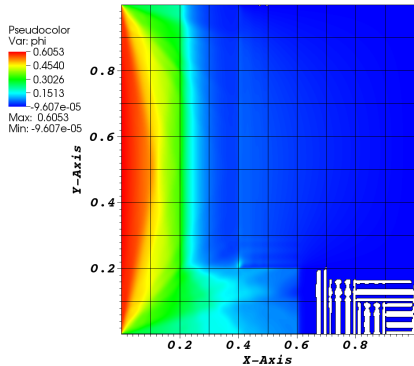
Material Region	$\sigma_t \text{ cm}^{-1}$	$\sigma_s \text{ cm}^{-1}$
Source	1.0	1.0
Very thin absorber	0.0001	0.0
Thick absorber	10.0	0.0
Very thick absorber	100.0	0.0
Very thick scatterer	1000.0	1000.0

- Designed to test optical thicknesses ranging several orders of magnitude
- Create anisotropic fluxes into scattering region

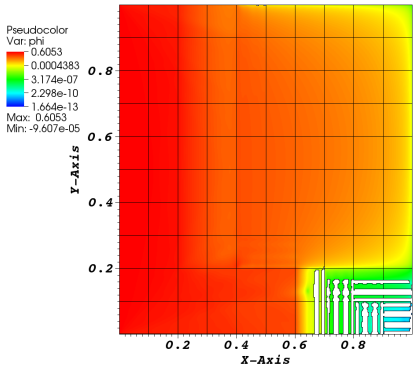


# X-Y Geometry

## Strong material heterogeneity problem results



Multi-material stress test solved with Robin BC MIP DSA. White regions indicate negative energy density.



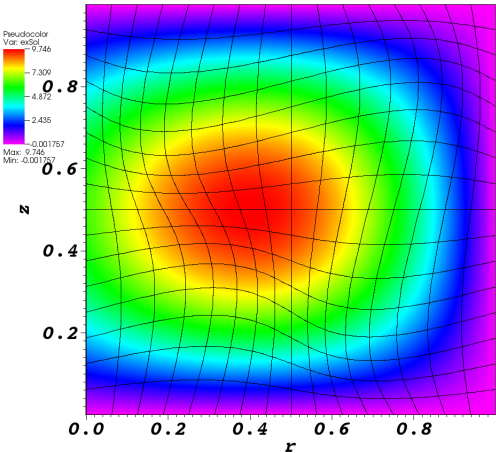
Log of multi-material stress test solved with Robin BC MIP DSA. White regions indicate negative energy density.

# R-Z Geometry

## MMS spatial convergence study

$$\psi_{\text{MMS}} = (\sin(\pi r) + 1 - r) \sin(\pi z)$$

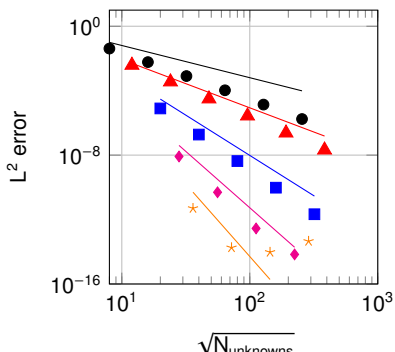
- Bailey et al. demonstrated 2<sup>nd</sup>-order convergence for PWL and BLD
- We solve using  $p = \{1, 2, 4, 6, 8\}$  on an orthogonal and 2<sup>nd</sup>-order curved mesh
- $S_8$  level-symmetric angular quadrature



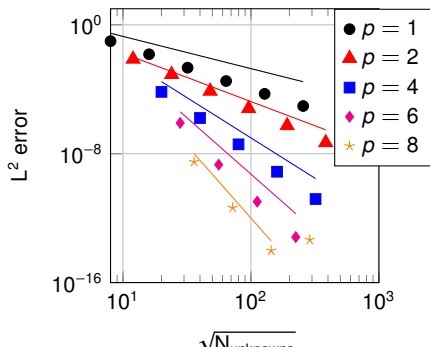
# R-Z Geometry

MMS spatial convergence study shows  $p + 1$  convergence

- $N_{\text{unknowns}} = N_{\text{cells}}(p + 1)^2$
- Reference lines show  $p + 1$  spatial convergences



Orthogonal mesh



2<sup>nd</sup>-order curved mesh

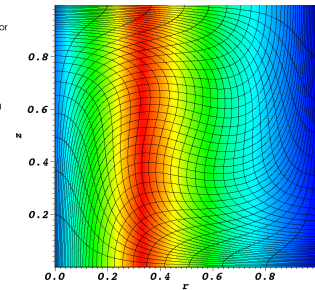
# R-Z Geometry

Regularity constrained spatial convergence study shows  $O(3/2)$  convergence rates

- Method of manufactured solutions (MMS) to determine convergence rates

$$\psi_{\text{MMS}} = \begin{cases} 1.0 + 4.0r, & 0 \leq r < 0.33 \\ 3.31 - 3.0r, & 0.33 \leq r < 0.66 \\ 2.32 - 1.5r, & r \leq 1.0 \end{cases}$$

- Calculate  $\|\phi_{\text{code}} - \phi_{\text{MMS}}\|_{L^2}$  for sequential mesh refinements
- Use  $p = \{1, 2, 4\}$ ,  $S_{12}$  level-symmetric angular quadrature, 2<sup>nd</sup>-order mesh



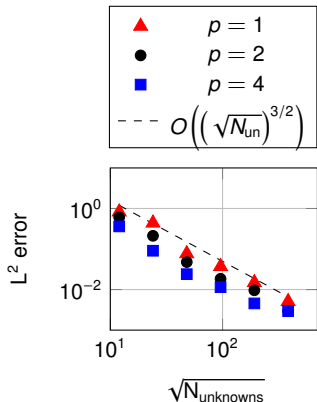
# R-Z Geometry

Regularity constrained spatial convergence study shows  $O(3/2)$  convergence rates

- Method of manufactured solutions (MMS) to determine convergence rates

$$\psi_{\text{MMS}} = \begin{cases} 1.0 + 4.0r, & 0 \leq r < 0.33 \\ 3.31 - 3.0r, & 0.33 \leq r < 0.66 \\ 2.32 - 1.5r, & r \leq 1.0 \end{cases}$$

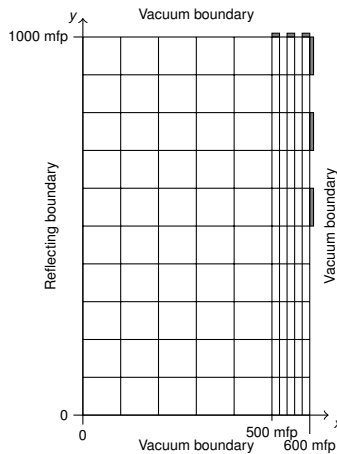
- Calculate  $\|\phi_{\text{code}} - \phi_{\text{MMS}}\|_{L^2}$  for sequential mesh refinements
- Use  $p = \{1, 2, 4\}$ ,  $S_{12}$  level-symmetric angular quadrature, 2<sup>nd</sup>-order mesh



# R-Z Geometry

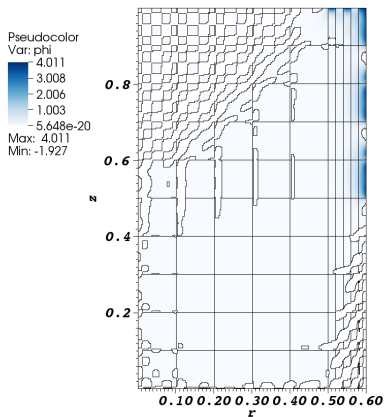
## Strong scatter with alternating boundary conditions

- Incident flux boundary at gray cells  
 $\psi_{\text{inc}} = 2/\pi$
- $\sigma_t = 1000, \sigma_s = 999, S_0 = 0$
- 4<sup>th</sup>-order finite elements
- Designed to reveal boundary layer

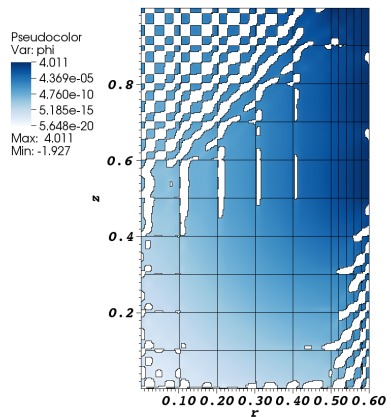


# R-Z Geometry

Strong scatter with alternating boundary conditions



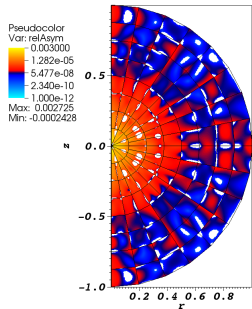
Scalar flux; white regions indicate negative scalar flux.



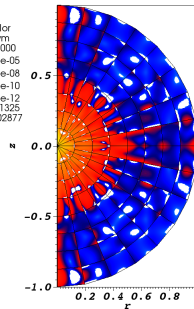
Log of scalar flux; white regions indicate negative scalar flux.

# Axisymmetry Preservation

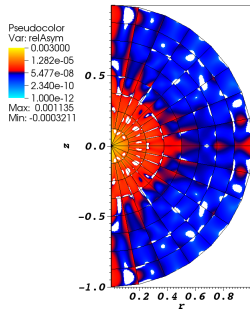
Relative asymmetry for 2<sup>nd</sup>-order finite elements on a 1<sup>st</sup>-order mesh for given order of level-symmetric angular quadrature



(a)  $S_4$



(b)  $S_8$

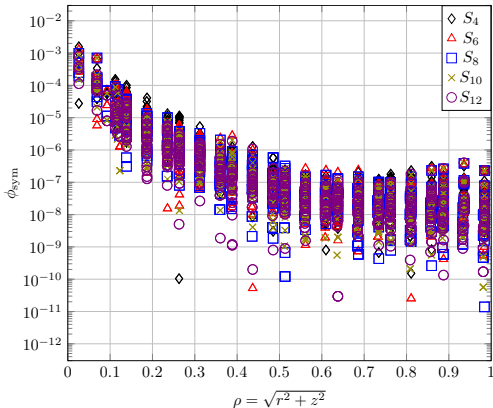


(c)  $S_{12}$

# Axisymmetry Preservation

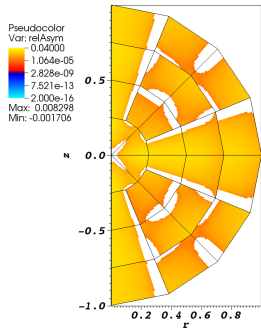
Relative asymmetry for 2<sup>nd</sup>-order finite elements on a 1<sup>st</sup>-order mesh for given order of level-symmetric angular quadrature

- Difficult to distinguish between  $S_N$  solutions
- Greatest asymmetry near origin
- Asymmetry reaches an asymptotic value  $\sim 10^{-7}$
- Accuracy of solution is nearly constant

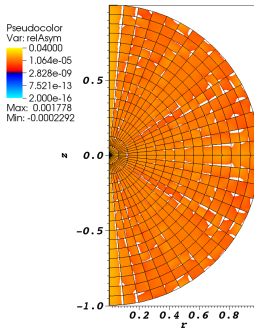


# Axisymmetry Preservation

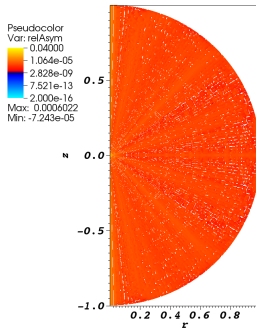
Relative asymmetry under spatial refinement for 1<sup>st</sup>-order finite elements on a 1<sup>st</sup>-order mesh for given order of level-symmetric angular quadrature



(a) 28 zones



(b) 496 zones

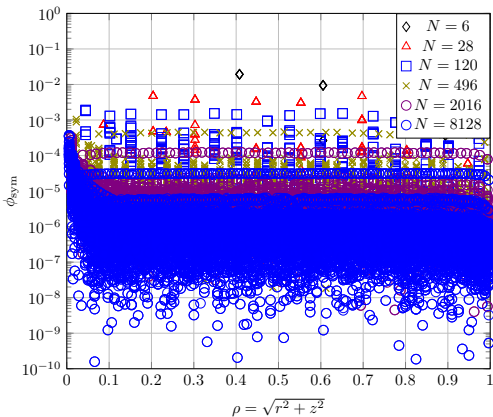


(c) 8128 zones

# Axisymmetry Preservation

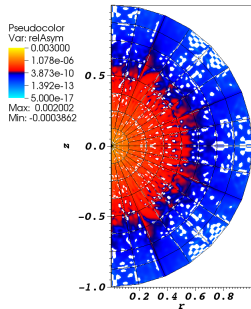
Relative asymmetries under spatial refinement for 1<sup>st</sup>-order finite elements on a 1<sup>st</sup>-order mesh for  $S_8$  level-symmetric angular quadrature

- Spatial refinement increases the symmetry preservation
- Bands appear from nodes near the z-axis
- Largest magnitude asymmetries are located near the origin

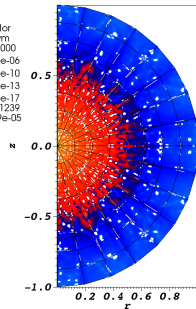


# Axisymmetry Preservation

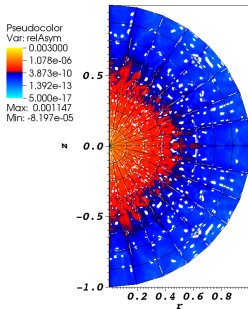
Relative asymmetry for 8<sup>th</sup>-order finite elements on a 1<sup>st</sup>-order mesh for given order of level-symmetric angular quadrature



(a)  $S_4$



(b)  $S_8$

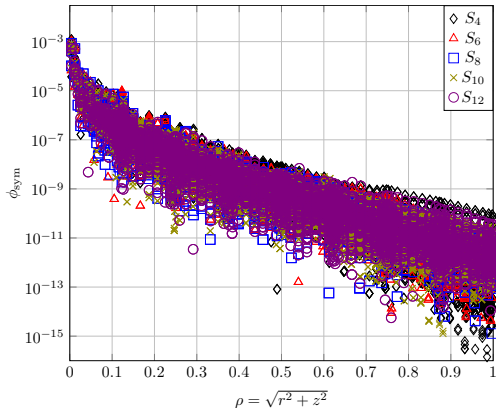


(c)  $S_{12}$

# Axisymmetry Preservation

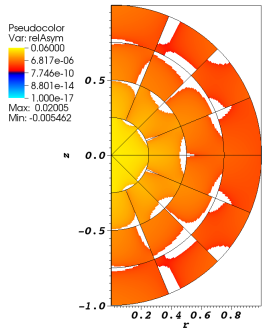
Relative asymmetry for 8<sup>th</sup>-order finite elements on a 1<sup>st</sup>-order mesh for given order of level-symmetric angular quadrature

- Difficult to distinguish between  $S_N$  solutions
- Greatest asymmetry near origin
- Asymmetry does not reach an asymptotic value ( $< 10^{-10}$ )
- Not a tremendous gain in symmetry compared to 4<sup>th</sup>-order finite elements
- Accuracy of solution is nearly constant

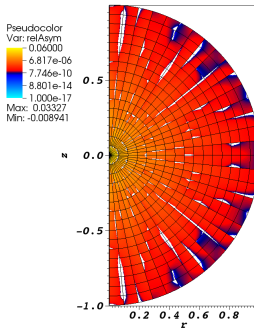


# Axisymmetry Preservation

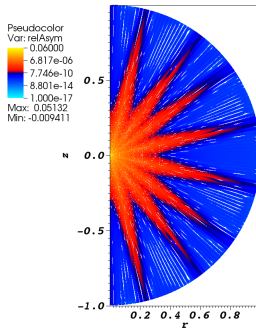
Relative asymmetry under spatial refinement for 1<sup>st</sup>-order finite elements on a 2<sup>nd</sup>-order mesh for given order of level-symmetric angular quadrature



(a) 28 zones



(b) 496 zones

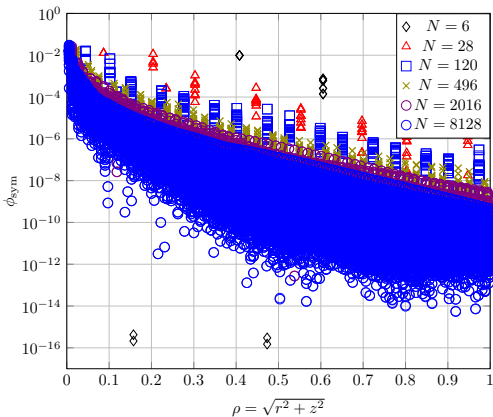


(c) 8128 zones

# Axisymmetry Preservation

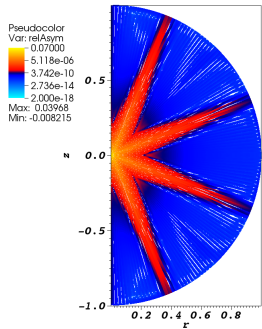
Relative asymmetries under spatial refinement for 1<sup>st</sup>-order finite elements on a 2<sup>nd</sup>-order mesh for  $S_8$  level-symmetric angular quadrature

- Spatial refinement increases the symmetry preservation
- Apparent “ray-effects”
- Largest magnitude asymmetries are located near the origin

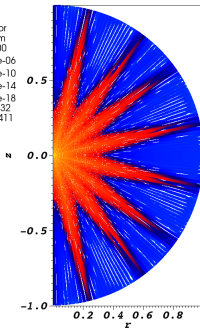


# Axisymmetry Preservation

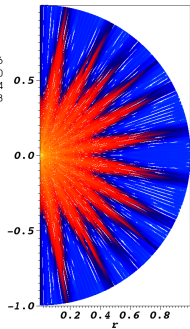
Relative asymmetry under spatial refinement for 1<sup>st</sup>-order finite elements on a 2<sup>nd</sup>-order mesh



(a)  $S_4$



(b)  $S_8$

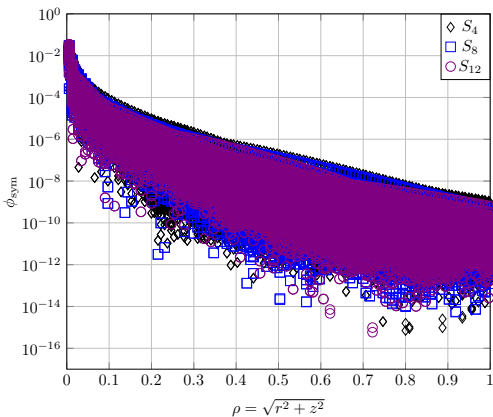


(c)  $S_{12}$

# Axisymmetry Preservation

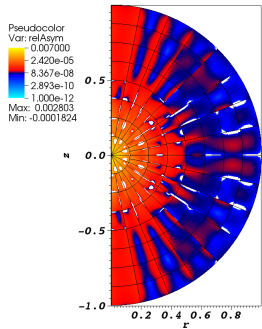
Relative asymmetries under spatial refinement for 1<sup>nd</sup>-order finite elements on a 2<sup>nd</sup>-order mesh for given level-symmetric angular quadrature

- Mesh refinement increases symmetry preservation
- Largest magnitude asymmetries are located near the origin

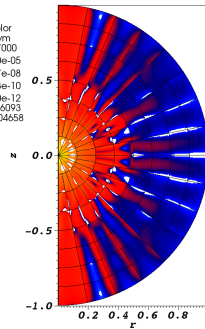


# Axisymmetry Preservation

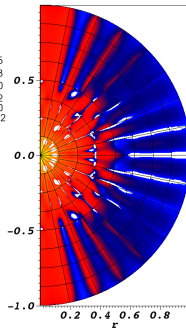
Relative asymmetry for 2<sup>nd</sup>-order finite elements on a 2<sup>nd</sup>-order mesh for given order of level-symmetric angular quadrature



(a)  $S_4$



(b)  $S_8$

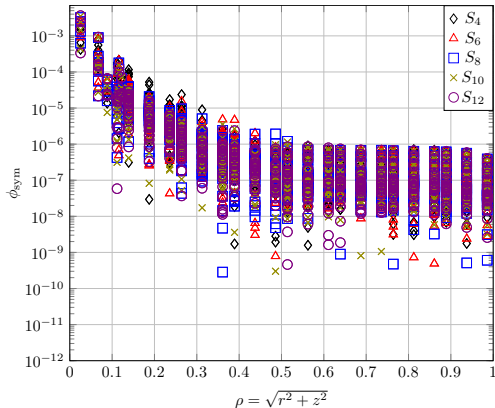


(c)  $S_{12}$

# Axisymmetry Preservation

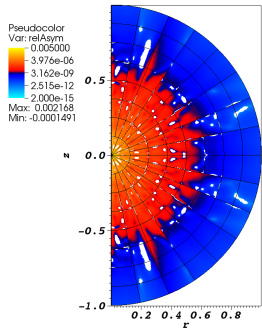
Relative asymmetry for 2<sup>nd</sup>-order finite elements on a 2<sup>nd</sup>-order mesh for given order of level-symmetric angular quadrature

- Difficult to distinguish between  $S_N$  solutions
- Greatest asymmetry near origin
- Large asymmetry on z-axis
- Asymmetry reaches an asymptotic value  $\sim 10^{-6}$
- Accuracy is nearly constant

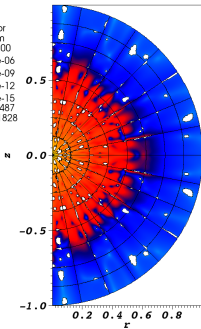


# Axisymmetry Preservation

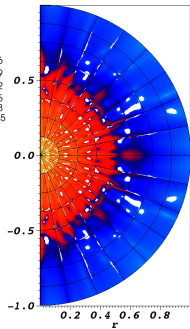
Relative asymmetry for 4<sup>th</sup>-order finite elements on a 2<sup>nd</sup>-order mesh for given order of level-symmetric angular quadrature



(a)  $S_4$



(b)  $S_8$

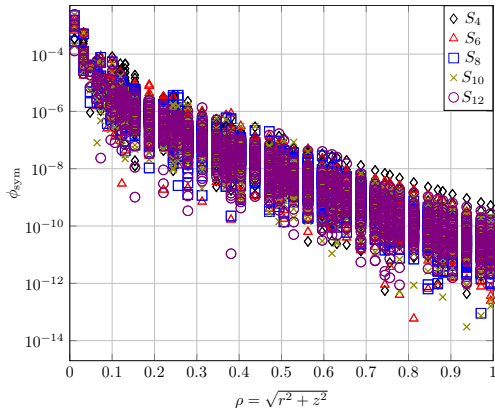


(c)  $S_{12}$

# Axisymmetry Preservation

Relative asymmetry for 4<sup>th</sup>-order finite elements on a 2<sup>nd</sup>-order mesh for given order of level-symmetric angular quadrature

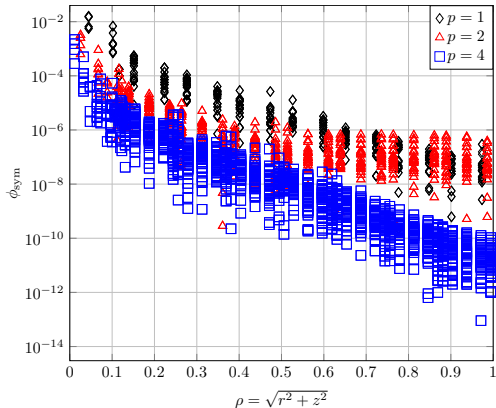
- Difficult to distinguish between  $S_N$  solutions
- Greatest asymmetry near origin
- Asymmetry does not reach an asymptotic value ( $< 10^{-9}$ )



# Axisymmetry Preservation

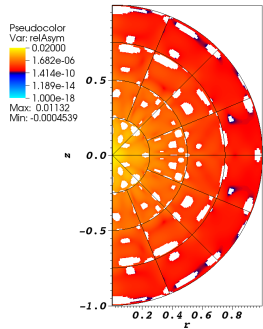
Relative asymmetries for each finite element order on a 2<sup>nd</sup>-order mesh for  $S_8$  level-symmetric angular quadrature

- 2<sup>nd</sup>-order finite elements reach a larger asymptotic asymmetry value
- Increasing finite element order increases relative symmetry
- Relative symmetry is similar at the origin

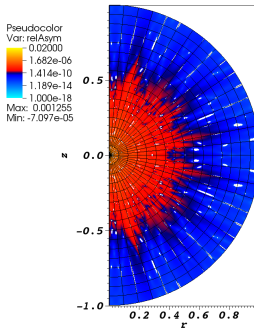


# Axisymmetry Preservation

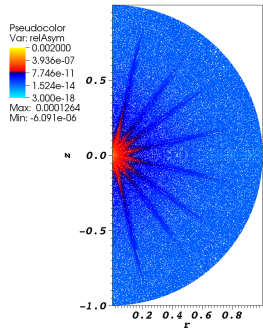
Relative asymmetry under spatial refinement for 4<sup>th</sup>-order finite elements on a 2<sup>nd</sup>-order mesh for given order of level-symmetric angular quadrature



(a) 28 zones



(b) 496 zones

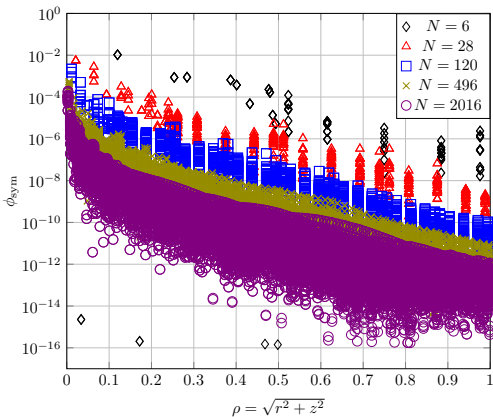


(c) 8128 zones

# Axisymmetry Preservation

Relative asymmetries under spatial refinement for 4<sup>st</sup>-order finite elements on a 2<sup>nd</sup>-order mesh for  $S_8$  level-symmetric angular quadrature

- Mesh refinement increases symmetry preservation
- Largest magnitude asymmetries are located near the origin



# Axysmmetry Preservation

MMS solution has strong gradient near the origin

$$\psi_{\text{MMS}}(r, z) = \rho$$

$$\equiv \sqrt{r^2 + z^2}$$

